1   **An ancient viral epidemic involving host coronavirus interacting genes**

2   **more than 20,000 years ago in East Asia**

3

4   Yassine Souilmi[1,2], M. Elise Lauterbur[3], Ray Tobler[1], Christian D. Huber[1], Angad S. Johar[1],

5   David Enard[3]

6

7   [1] Australian Centre for Ancient DNA, School of Biological Sciences, University of Adelaide,

8   Adelaide, SA 5005, Australia.

9   [2] National Centre for Indigenous Genomics, Australian National University, Canberra, ACT

10   0200, Australia.

11   [3] University of Arizona Department of Ecology and Evolutionary Biology, Tucson, Arizona, USA.

12

Summary

The current SARS-CoV-2 pandemic has emphasized the vulnerability of human
populations to novel viral pressures, despite the vast array of epidemiological and
biomedical tools now available. Notably, modern human genomes contain evolutionary
information tracing back tens of thousands of years, which may help identify the viruses
that have impacted our ancestors – pointing to which viruses have future pandemic
potential. Here, we apply evolutionary analyses to human genomic datasets to recover
selection events involving tens of human genes that interact with coronaviruses,
including SARS-CoV-2, that likely started more than 20,000 years ago. These adaptive
events were limited to the population ancestral to East Asian populations. Multiple lines
of functional evidence support an ancient viral selective pressure, and East Asia is the
geographical origin of several modern coronavirus epidemics. An arms race with an
ancient coronavirus, or with a different virus that happened to use similar interactions as
coronaviruses with human hosts, may thus have taken place in ancestral East Asian
populations. By learning more about our ancient viral foes, our study highlights the
promise of evolutionary information to better predict the pandemics of the future.
Importantly, adaptation to ancient viral epidemics in specific human populations does
not necessarily imply any difference in genetic susceptibility between different human
populations, and the current evidence points toward an overwhelming impact of
socioeconomic factors in the case of COVID-19.

Introduction

In the past 20 years, strains of the beta coronavirus genus (family Coronaviridae; Richman et
al., 2020) have been behind three major zoonotic outbreaks with grave impacts for human
populations (Ou et al., 2020). The first outbreak, commonly known as SARS-CoV (Severe Acute
Respiratory Syndrome), originated in China in late 2002 and eventually spread to 30 additional
counties where it infected more than 8,000 people and claimed nearly 800 lives (Hoffmann and
Kamps, 2003). Four years later, MERS-CoV (Middle East respiratory syndrome coronavirus)
affected >2,400 people and caused over 850 deaths, mostly in Saudi Arabia (World Health

2

42   Organization, 2019). The most recent outbreak began in late 2019 when SARS-CoV-2 – a less

43   virulent but far more contagious strain than those behind the two previous epidemics – emerged

44   in mainland China before spreading rapidly across the rest of the world, triggering an ongoing

45   pandemic (COVID-19) that so far has infected 45 million people and resulted in over one million

46   deaths worldwide (Dong et al., 2020).

47   The devastation caused by SARS-CoV-2 has inspired a worldwide research effort to develop

48   new vaccines and strategies that aim to curb its impact by determining the factors that underlie

49   its epidemiology. The resulting research has revealed that socioeconomic (e.g. access to

50   healthcare and testing facilities or exposure at work), demographic (e.g. population density and

51   age structure), and personal health factors all play a major role in SARS-CoV-2 epidemiology

52   (Balogun et al., 2020; Sattar Naveed et al., 2020; Scarpone et al., 2020). Additionally, several

53   genetic loci that mediate SARS-CoV-2 susceptibility and severity have been found in

54   contemporary European populations (Ellinghaus et al., 2020; Roberts et al., 2020), one of which

55   contains a genetic variant that increases SARS-CoV-2 susceptibility that likely increased in

56   frequency in the ancestors of modern Europeans after interbreeding with Neanderthals ~40,000

57   years ago (Zeberg and Pääbo, 2020). This historical admixture event has led to genetic

58   differences within and between contemporary human populations that directly impact COVID-19

59   epidemiology – the Neanderthal-derived variant haplotype is now carried by 8% of modern

60   Europeans, but at lower frequencies in African populations whose ancestors did not experience

61   this admixture event – and suggests that evolutionary analyses of human populations may help

62   reveal these genetic differences and ultimately assist in the development of novel drugs and

63   therapies to combat the negative impacts of SARS-CoV-2.

64   Throughout the evolutionary history of our species, positive natural selection has frequently

65   targeted proteins that physically interact with viruses – e.g. those involved in immunity, or used

66   by viruses to hijack the host cellular machinery (Barreiro et al., 2009; Enard et al., 2016; Sawyer

67   et al., 2005). In the ~6 million years since the ancestors of humans and chimpanzees

68   separated, selection has led to the fixation of gene variants encoding virus-interacting proteins

69   (VIPs) at three times the rate observed for other classes of genes (Enard et al., 2016; Uricchio

70   et al., 2019). Moreover, strong selection on VIPs has continued in human populations during the

71   past 50,000 years, as evidenced by VIP genes being enriched for adaptive introgressed

72   Neanderthal variants and also selective sweep signals (i.e. selection that drives a beneficial

73   variant to substantial frequencies in a population), particularly around VIPs that interact with

74   RNA viruses, a viral class that includes the coronaviruses (Enard and Petrov, 2018, 2020).

75   The accumulated evidence suggests that ancient RNA virus epidemics have occurred frequently

76   during the history of our species; however, we currently do not know if selection has made a

77   substantial contribution to the evolution of human genes that interact more specifically with

78   coronaviruses.

79   Accordingly, here we investigate whether ancient coronavirus epidemics have driven past

80   adaptation within and across modern human populations, by examining if selection signals are

81   enriched within a set of 420 VIPs that interact with coronaviruses (denoted CoV-VIPs; Table S1)

82   across 26 worldwide human populations from the 1000 Genomes Project (1000 Genomes

83   Project Consortium, 2015). These CoV-VIPs comprise 332 SARS-CoV-2 VIPs that were

84   recently identified by high-throughput mass spectrometry (Gordon et al., 2020) and an additional

85   88 proteins that were manually curated from the coronavirus literature (e.g. SARS-CoV-1,

86   MERS, HCoV-NL63, etc; Table S1; Enard and Petrov, 2018), and form part of a larger set of

87   5,291 previously published VIPs (SI; Table S1) from multiple viruses known to infect humans

88   (Enard and Petrov, 2018). Our focus upon host adaptation at VIPs is motivated by evidence

89   indicating that these protein interactions are the central mechanism that viruses use to hijack

90   the host cellular machinery, as shown by the strong focus of virologists on these interactions

91   (Enard and Petrov, 2018). Accordingly, VIPs are much more likely to have functional impacts on

92   viruses than proteins not known to interact with viruses (see SI: *Host adaptation is expected at*

93   *VIPs*). Our enrichment-based approach is expected to be particularly powerful if the ancestors

94   of one or more of the 26 modern human populations were exposed to epidemics driven by

95   coronavirus-like viruses that resulted in selection upon multiple CoV-VIPs (see Discussion). An

96   alternative that we cannot exclude however is that a different type of virus that happens to use

97   similar VIPs as coronaviruses might instead create an enrichment in adaptation signals at CoV-

98   VIPs.

99   Our analyses of CoV-VIPs find a strong enrichment in sweep signals in these proteins across

100   multiple East Asian populations, which is absent from other human populations. This suggests

101   that an ancient coronavirus epidemic (or another virus using similar VIPs) drove an adaptive

102   response in the ancestors of East Asians, which is in agreement with the current geographic

103   range of the major known animal reservoirs of coronaviruses (Wong et al., 2019). Further, by

104   leveraging ancestral recombination graph approaches (Speidel et al., 2019; Stern et al., 2019)

105   we find that amongst the putatively selected CoV-VIPs, 42 first may have come under selection

106   around 900 generations (~25,000 years, most likely 20,000 years ago or more) ago and exhibit

107   a coordinated adaptive response that lasted until around 200 generations (~5,000 years) ago.

108   By drawing upon other publicly available datasets, we show that the CoV-VIP genes are

109   enriched for anti- and proviral effects and variants that affect COVID-19 etiology in the modern

110   European British population (https://grasp.nhlbi.nih.gov/Covid19GWASResults.aspx). We

111   nevertheless do not investigate in which particular direction, as we cannot expect the British

112   population to be representative of East Asian populations in that respect. We further show that

113   the inferred underlying causal mutations are situated near to regulatory variants active in lungs

114   and other tissues negatively impacted by COVID-19. Taken together, these independent lines of

115   evidence provide support for an ancient coronavirus (or another virus that was using similar

116   interactions) epidemic that emerged more than 20,000 years ago in the ancestors of

117   contemporary East Asian populations, whose genetic signature remains apparent in the

118   genomes of the present-day populations now living in this region.

Results

## Signatures of adaptation to an ancient epidemic

121   Viruses have exerted strong selective pressures on the ancestors of modern humans (Enard

122   and Petrov, 2020; Uricchio et al., 2019). Accordingly, we use two population genetic statistical

123   tests that are sensitive to such genetic signatures (i.e. selective sweeps) – nSL (Ferrer-Admetlla

124   et al., 2014) and iHS (Voight et al., 2006) – and which are able to detect genomic regions

125   impacted by strong selection across a wide range of parameters (e.g. different starting and end

126   frequencies of the selected allele). Both statistics also have the advantage of being insensitive

127   to background selection (Enard et al., 2014; Schrider, 2020), thereby reducing the potential

128   impact of false positives in our analyses.

129   After scanning each of the 26 populations for signals of selection, we apply an enrichment test

130   that was previously used to detect enriched selection signals in RNA VIPs in human populations

131   (Enard and Petrov, 2020). Briefly, for each population and selection statistic, we rank all genes

132   based on the average selection statistic score observed in genomic windows ranging from 50kb

133   to 2Mb (Methods). Different windows sizes are used because smaller windows tend to be more

134   sensitive to weaker sweeps, whereas larger windows tend to be more sensitive to stronger

135   sweeps (Enard and Petrov, 2020; Methods). After ranking the gene scores, we estimate an

136   enrichment curve (Figure 1) for gene sets ranging from the top 10 to 10,000 ranked loci

137   (Methods). The significance of the whole enrichment curve is then calculated using a genome

138   block-randomization approach that accounts for the genomic clustering of neighboring CoV-

139 VIPs, and provides an unbiased false positive risk for the whole enrichment curve (FPR) by re-

140 running the entire enrichment analysis pipeline on block-randomized genomes (Enard and

141 Petrov, 2020; Methods). For our control gene set, we use protein-coding genes situated at least

142 500kb from CoV-VIPs to avoid overlapping the same sweep signals. Additionally, genes in the

143 control sets are chosen to have similar characteristics as the CoV-VIPs (e.g. similar

144 recombination rates, density of coding and regulatory sequences, percentage of immune genes,

145 percentage of genes that interact with bacteria; see Methods for the complete list of factors) to

146 ensure that any detected enrichment is virus-specific rather than due to a confounding factor

147 (Enard and Petrov, 2020). Choosing controls far away and that match multiple potential

148 confounding factors has the effect of shrinking the pool of potential control genes, which can

149 affect the variance and also the representativity of this pool as a null control. The possible

150 impacts of the size of the control pool are however fully taken into account in the FPR estimated

151 with block-randomized genomes (Enard and Petrov, 2020; Methods). Finally, we also exclude

152 the possibility that functions other than viral interactions might explain our results by running a

153 Gene Ontology analysis (Gene Ontology Consortium, 2015; SI; Tables S2, S3 and Figure S1).

154 Applying this approach to each of the 26 human populations from the 1,000 genomes dataset,

155 we find a very strong enrichment of sweep signals in CoV-VIPs across all top-ranked gene set

156 sizes that is specific to the five East Asian populations (whole enrichment curve for nSL and iHS

157 combined FPR=2.10^{-4}; Figures 1 & S2; Methods). No enrichment is observed for populations

158 from other continental regions, including in neighboring South Asia (whole enrichment curve for

159 nSL and iHS combined FPR>0.05 in all cases; Figures 1 & S2). Further, no enrichment is

160 detected for VIP sets for 17 other viruses in East Asian populations (whole enrichment curve for

161 nSL and iHS separately or combined, P>0.05 in all cases; Figures S3 & S4). Taken together,

162 these results suggest that coronaviruses, or another type of viruses that used similar

163 interactions with human hosts, have driven ancient epidemics in ancient human populations that

164 are ancestral to modern East Asians. This enrichment is unlikely to have been caused by any

165 other virus represented in our set of 5,291 VIPs, but we still cannot exclude that a currently

166 unknown type of virus that happened to use similar VIPs as coronaviruses could have been

167 involved instead (Table S1). The enrichment is most substantial for the top-ranked gene sets

168 ranging between the top 10 and top 1,000 loci (Figure 1; whole enrichment curve FPR=3.10^{-6} for

169 nSL, FPR=4.10^{-3} for iHS, FPR=6.10^{-5} for iHS and nSL combined), and is particularly strong for

170 the top 200 loci in large windows (1 Mb) where a four-fold enrichment is observed for both nSL

171 and iHS statistics (pertaining to between 10 to 13 selected CoV-VIPs amongst the top 200

172   ranked genes; Table S4). This suggests that strong selection targeted multiple CoV-VIPs in the

173   common ancestors of modern East Asian populations. That the selected haplotype structures

174   are detected by both the iHS and nSL methods suggests that they are unlikely to have occurred

175   prior to 30,000 years ago, as both nSL and iHS have little power to detect adaptive events

176   arising before this time point in human evolution (Sabeti et al., 2006)

177

178
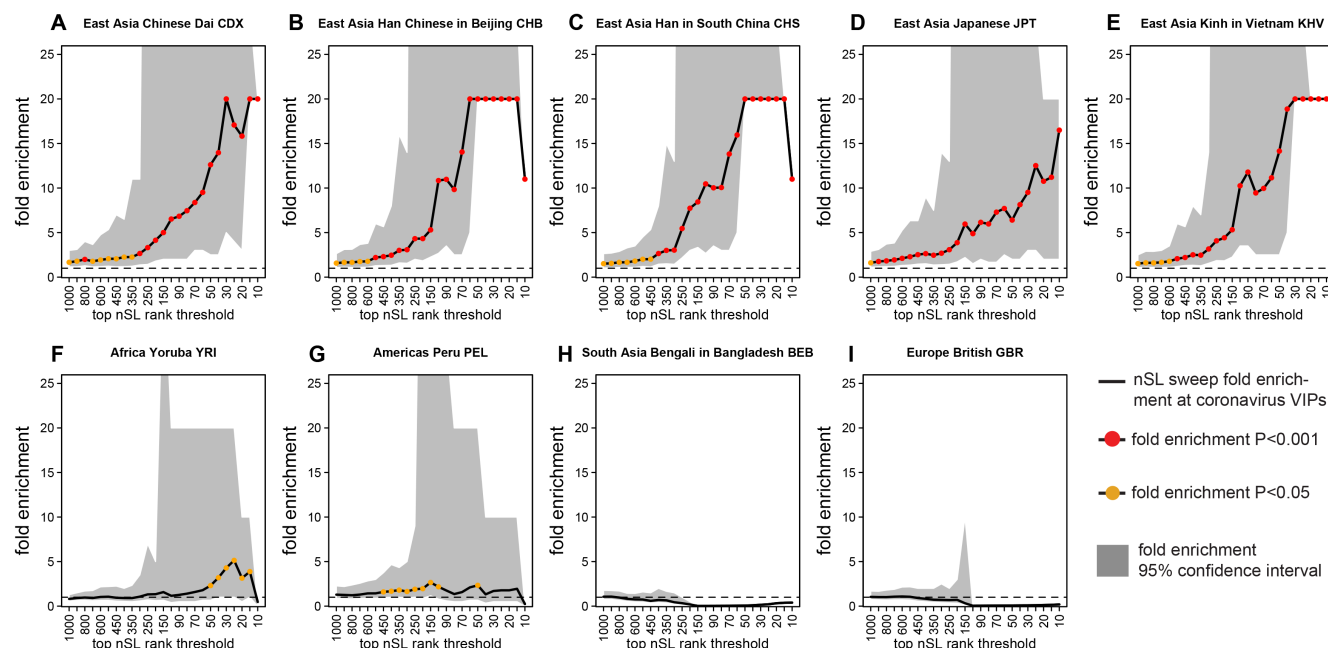
180 **Figure 1. Coronavirus VIPs nSL ranks enrichment**

181 A,B,C,D,E are East Asian populations, F,G,H,I are populations from other continents. The y axis

182 represents the bootstrap test (Methods) relative fold enrichment of the number of genes in

183 putative sweeps at CoV-VIPs, divided by the number of genes in putative sweeps at control

184 genes matched for multiple confounding factors. The x axis represents the top rank threshold to

185 designate putative sweeps. Black full line: average fold enrichment over 5,000 bootstrap test

186 control sets. Fold enrichments greater than 20 are represented at 20. Grey area: 95%

187 confidence interval of the fold enrichment over 5,000 bootstrap test control sets. The rank

188 thresholds where the confidence interval lower or higher fold enrichment has a denominator of

189 zero are not represented (For example, graph B, top 10 rank threshold). Lower confidence

190 interval fold enrichments higher than 20 are represented at 20 (for example, graph B, top 30

191 rank threshold). Red dots: bootstrap test fold enrichment P<0.001. Orange dots: bootstrap test

192 fold enrichment P<0.05. Note that the bootstrap test p-values are not the same as the whole

193 curve enrichment false positive risk (FPR) estimated using block-randomized genomes on top of

194 the bootstrap test (Methods).

7

An ancient epidemic in the ancestors of East Asians starting more than 20,000 years ago

To further test the existence of an ancient viral epidemic in the ancestors of East Asians, we use a recent ancestral recombination graph (ARG)-based method, Relate (Speidel et al., 2019), to infer the timing and trajectories of selected loci for the CoV-VIPs. If the selective pressure responsible for the multiple independent selection events at CoV-VIPs was relatively sudden as expect from a new epidemic, then these selection events should have started independently around the same time. By estimating ARGs at variants distributed across the entire genome, Relate can reconstruct coalescent events across time and detect genomic regions impacted by positive selection, while explicitly controlling for historical variation in population demography. To approximate the start time of selection, Relate estimates the first historical time point that a putatively selected variant had an observable frequency unlikely to be equal to zero (Methods). We use this approximation as the likely starting time of selection, although we note that this method does not account for selection on standing variants that had non-zero frequencies at the onset of selection (Methods). Additionally, we use the iSAFE software – which enables the localization of selected mutations (Akbari et al., 2018) – along with a curated set of regulatory variants (expression QTLs; eQTLs) from the eGTEx Project (2017) to help identify the likely causal mutations in the selected CoV-VIP genes. There is good evidence that the majority of adaptive mutations in the human genome are regulatory mutations (Enard et al., 2014; Kudaravalli et al., 2009; Nédélec et al., 2016; Quach et al., 2016) and, accordingly, we find that iSAFE peaks are significantly closer to GTEx eQTLs proximal to CoV-VIP genes than expected by chance (iSAFE peak proximity test, $P<10^{-9}$; Methods). Therefore, for each CoV-VIP gene, we choose a variant with the lowest Relate p-value ($<10^{-3}$; Methods) that is situated at or close to a GTEx eQTL associated with the focal gene to estimate the likely starting time of selection for that gene (Methods; Figure S5).

Using this approach, we observe 42 CoV-VIPs (Table S5 and Figure S5) with selection starting times clustered around a peak 870 generations ago (~200 generations wide, potentially due to noise in our estimates; Figure 2). While this amounts to about four times more selected CoV-VIP genes than were detected using either nSL or iHS (both detected around ten CoV-VIPs amongst the top 200 ranked genes; Table S4) this is not unexpected as Relate has more power to detect selection events than nSL and iHS when the beneficial allele is at intermediate frequencies at the point of measurement (typically <60%; Figure 3; Enard and Petrov, 2020; Ferrer-Admetlla et al., 2014; Voight et al., 2006). The relatively tight temporal clustering of starting times forms a highly significant peak (peak significance test $P=2.3.10^{-4}$; Figure 2) when

8

228   comparing the observed clustering of CoV-VIPs start times with the distribution of inferred start

229   times for randomly sampled sets of genes (Methods). Note that this peak significance test is

230   gene clustering-aware (Methods). Further, this significance test is not biased by the fact that

231   CoV-VIPs are enriched for sweep signals, as the test remains highly significant (P=1.10^{-4}) when

232   using random control sets with comparable high-scoring nSL statistics (Methods). This suggests

233   that the tight temporal clustering of selection events is a specific feature of the CoV-VIPs, rather

234   than a confounding aspect of any gene set similarly enriched for sweeps.

235
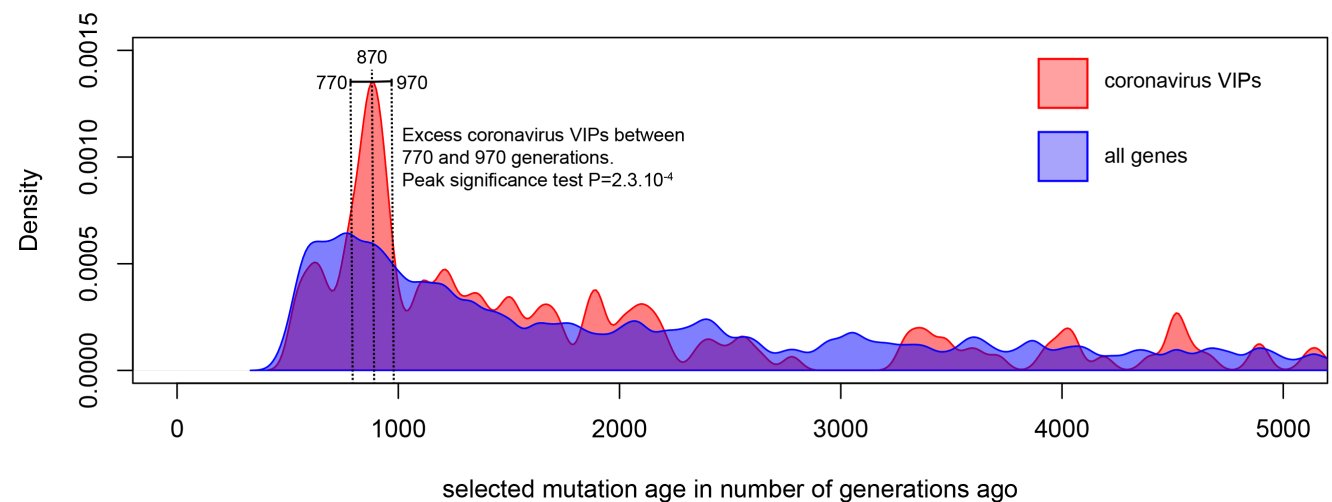
Figure 2. Timing of selection at CoV-VIPs
The figure shows the distribution of selection start times at CoV-VIPs (pink distribution)
compared to the distribution of selection start times at all loci in the genome (blue distribution).
Details on how the two distributions are compared by the peak significance test, and how the
selection start times are estimated with Relate, are provided in Methods.

242   The genes with clustered selection starting times around 900 generations ago are enriched in

243   strong nSL signals, as shown by running the peak significance test using only CoV-VIPs and

244   controls with strong nSL signals (Figure S6). Conversely, the peak disappears when restricting

245   this test to weaker nSL signals (P=0.53 when using the lowest 50% of nSL statistics; Methods).

246   Importantly, our estimates of the timing of selection are not biased by our use of methods that

247   rely on selected variants not being fixed in the population at the time of genome sampling (i.e.

248   Relate). When rerunning our analytical pipeline focusing only on strong candidate loci according

249   to Tajima's D (Tajima, 1989), a statistic developed to detect recently completed sweeps (i.e.

250   fixed mutations), we observe the same clustering of selection events starting around 900

251   generations ago (Figure S7). Further, the remaining 382 CoV-VIPs that are not part of this

252   temporal cluster around 900 generations ago are not more likely to have significant Tajima's D

253   values than controls (whole enrichment curve P=0.07). Consequently, our results are consistent

254   with the emergence of a viral epidemic ~900 generations, or ~25,000 years (900 generations *

255   28 years per generation; Moorjani et al., 2016), ago that drove a burst of strong positive

256   selection in the ancestors of East Asians, which may represent a genetic record of a multi-

257   generational viral epidemic amongst the 26 human populations tested here.

258   Although selective pressures other than a coronavirus or another unknown type of virus with

259   similar host interactions might also contribute to these patterns, we note that the signal is

260   restricted specifically at CoV-VIPs and none of 17 other viruses that we tested exhibit the same

261   temporal clustering ~900 generations ago in East Asia (peak significance test P>0.05 in all

262   cases; Methods). Further, this test remained highly significant when retesting the temporal

263   clustering of CoV-VIPs using only other RNA VIPs as the control set (P=4.10^{-4}; Table S1),

264   consistent with the clustered selection signals being a coordinated adaptive response to a

265   coronavirus or another virus using similar host interactions.

266

267   **Strong selection drove coordinated changes in multiple CoV-VIP genes over 20,000 years**

268   To learn more about the likely start and duration of the selection pressure acting on the

269   ancestors of East Asians, we use CLUES (Stern et al., 2019) to infer allele frequency

270   trajectories and selection coefficients for the inferred beneficial mutations proximal to the 42

271   CoV-VIP genes with selection starting 900 generations ago according to Relate (Figure 3).

272   CLUES uses the temporal variation in population size and coalescence rates inferred by Relate

273   to reconstruct frequency trajectories while taking demographic fluctuations into account. Our

274   observation of sweep signals at 42 CoV-VIP genes in the ancestors of East Asians suggests

275   that the putative underlying viral epidemic likely spanned many generations (i.e. the time

276   needed for selection to drive initially rare alleles to intermediate/high frequencies). Accordingly,

277   we anticipate that selection was probably strongest when the naive host population was first

278   infected by the virus, before gradually waning as the host population adapted to the viral

279   pressure (Hayward and Sella, 2019). Similarly, a decrease in the virulence of the virus over

280   time, a phenomenon that has been reported during the long term bouts of host-virus coevolution

281   (Best and Kerr, 2000), would also result in the gradual decrement of selection coefficients

282   across time. Hence, for each of the 42 CoV-VIPs predicted to have started coming under

283   selection ~900 generations ago, we use CLUES to estimate the selection coefficient in two

284   successive time-intervals (between 1,000 and 500 generations ago, and from 500 generations

285   ago to the present), predicting that selection would be stronger in the oldest interval. We note

286   that a 500 generations interval was reported as the approximate timespan that CLUES provides

287   reliable estimates for humans (Stern et al., 2019); using smaller generations intervals, we would

288   run the risk of getting overly noisy selection coefficient estimates based on too few coalescent

289   events. However, 500 generations intervals are not adequate to obtain reasonable estimates of

290   the precise duration of the selective pressure (Stern et al., 2019), so we do not attempt to

291   estimate this parameter here, and we simply try to compare the two time periods with each

292   other. Also, because CLUES uses a computationally intensive algorithm when following the

293   recommendations of Stern et al. (2020), we base our estimates on only two of the five East

294   Asian populations (i.e. Dai and Beijing Han Chinese; Figure 3A, B and 3C, D, respectively).
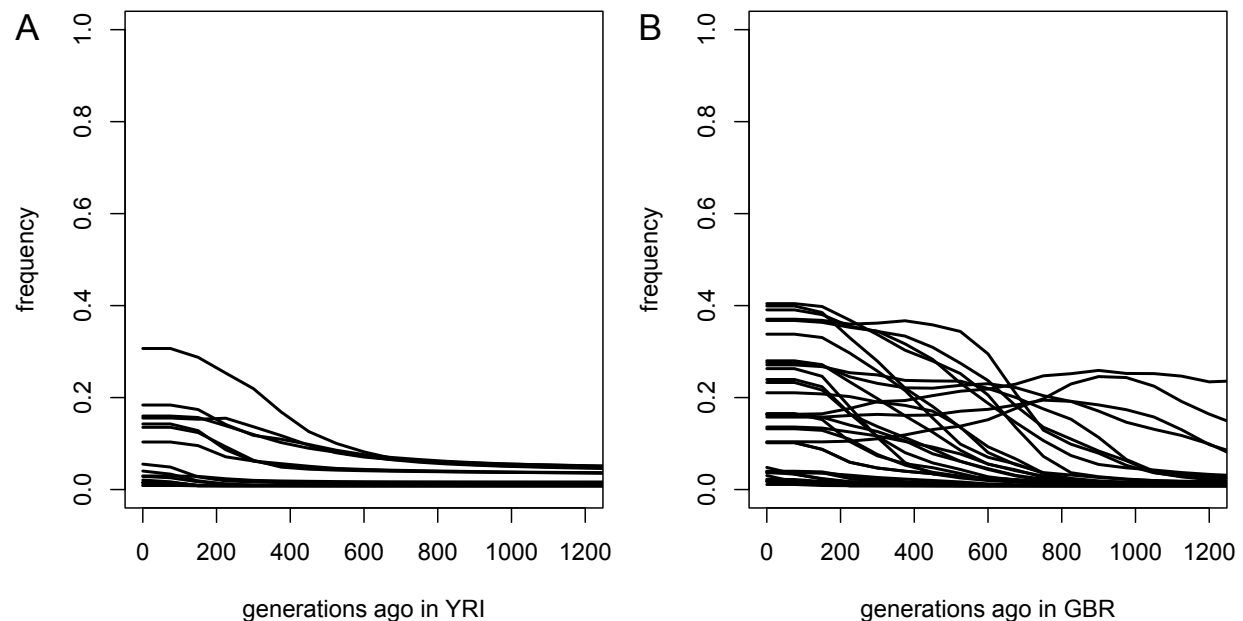
295   CLUES infers frequency trajectories that are more complex than a simple, clear, abrupt jump in

296   frequency 900 generations ago. Instead, the estimated frequency trajectories (Figure 3A,B,C,D)

297   suggest that 900 generations ago is the approximate time when the bulk of the selected variants

298   reached a frequency of a few percent or more, and approximately when there is an acceleration

299   in the frequency increase (Figure 3B, D). This might correspond to the transition between the

300   establishment and exponential phases of the sweeps, and might imply that the selective

301   pressure is older than 900 generations. The initially flatter, slower increases in frequency,

302   lasting sometimes up to 600 generations ago for some variants, are compatible with either co-

303   dominant or recessive alleles, and likely exclude dominant alleles that would start increasing in

304   frequency more abruptly. Interestingly, this would be in good agreement with the rarity of

305   dominant eQTLs in GTEx, if selected variants were indeed regulatory (GTEx Project, 2017).

306   Although the flat, slow starts of frequency increases make it hard to pinpoint when selection

307   started exactly, the vast majority of the selected alleles appear to have reached 5% or higher

308   frequencies by 600 generations, thus making it highly unlikely that the selective pressure would

309   have started 600 or less generations ago. Frequency trajectories estimated in the Yoruba

310   African population (Figure 4A) or the British European population (Figure 4B) also show very

311   low frequencies 900 generations ago. The selected variants in East Asia are found nowadays at

312   very low frequencies especially in Africa (Table S6). This implies that they are substantially

313   older than when selection started in East Asia, which may then be described as selection on low

314   frequency standing variation. Intriguingly, some variants rise in frequency (up to 40% frequency

315   at most) in Europe mostly after 800 generations ago. A small number of variants in Africa

316   increase in frequency (up to 30% frequency at most) after 600 generations ago.

317   The selected mutations are estimated to have continually increased in frequency in East Asia

318   until ~200 generations (approximately 5,000 years) ago, after which they remained relatively

319   stable (Figure 3A, C). Accordingly, CLUES estimates very high selection coefficients in the

320   interval between 1,000 and 500 generations ago (Dai average s = 0.034, Beijing Han average s

321   = 0.042; Figure 5A, B), but much weaker selection coefficients from 500 generations ago up to

322   the present (Dai average s = 0.002, Beijing Han average s = 0.003; Figure 5A, B). These

323   patterns are consistent with the appearance of a strong selective pressure that triggered a

324   coordinated adaptive response across multiple independent loci, which waned through time as

325   the host population adapted to the viral pressure and/or as the virus became less virulent.

326
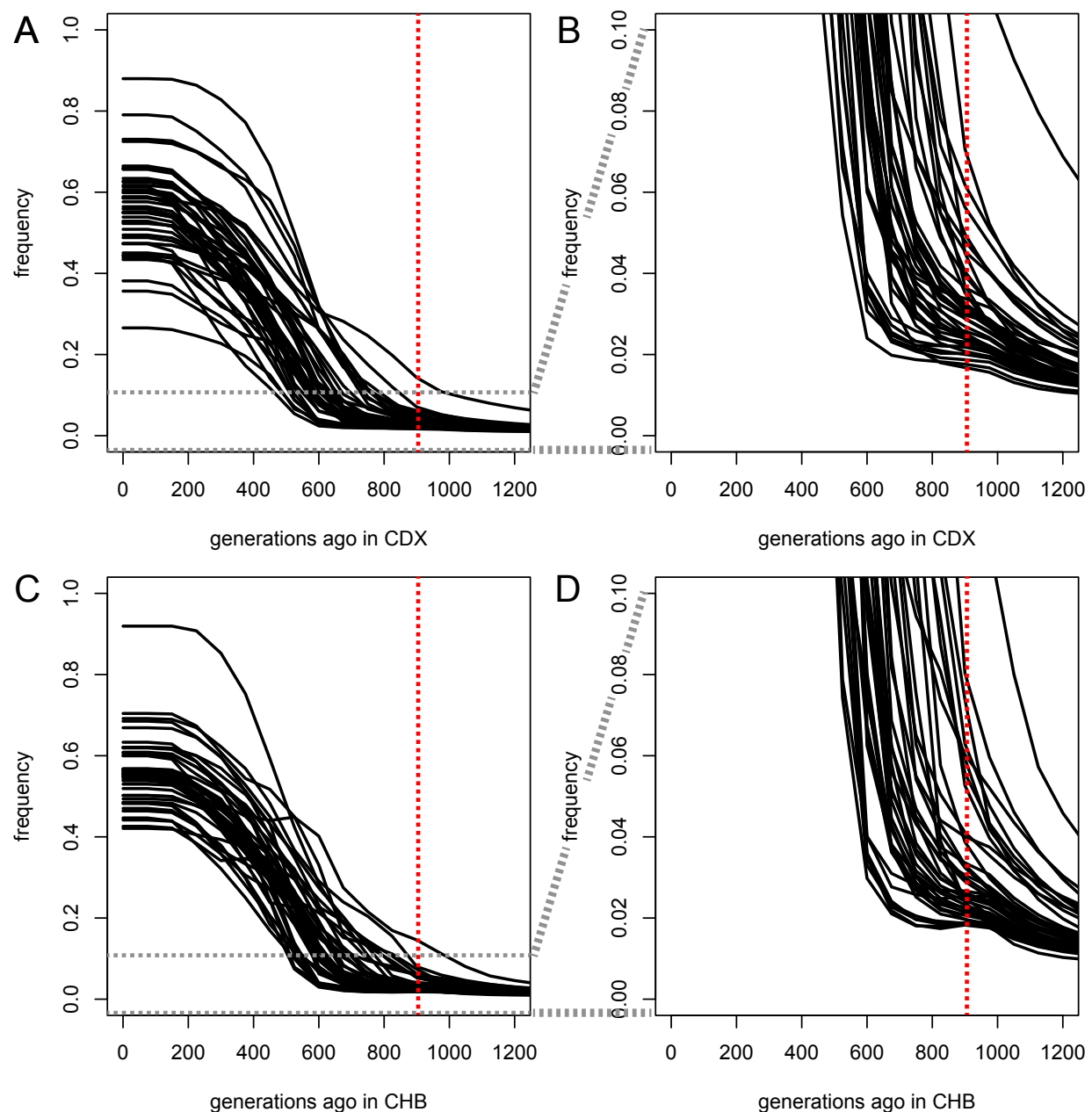
**Figure 3. Selected CoV-VIPs allele frequency trajectories over time estimated by CLUES in East Asia**

Each frequency trajectory is for one of the 42 Relate selected mutations at CoV-VIPs within the peak around 900 generations ago (Methods). A) Frequency trajectories in the Chinese Dai CDX 1,000 Genomes population. B) Same, but zoomed-in from frequencies 0 to 10%. C) Frequency trajectories in the Han Chinese from Beijing CHB 1,000 Genomes population. D) Same, but zoomed-in from frequencies 0 to 10%.

13

Figure 4. Selected CoV-VIPs allele frequency trajectories over time estimated by CLUES in Africa (Yoruba) and Europe (British)
Same as Figure 3. A) Yoruba population. The graph includes 17 frequency trajectories, the 25 other alleles selected in East Asia being absent in the Yoruba sample (but not Africa overall, see Table Sx) B) British population. The graph includes 35 frequency trajectories, the other seven alleles selected in East Asia being absent in the British sample.

14
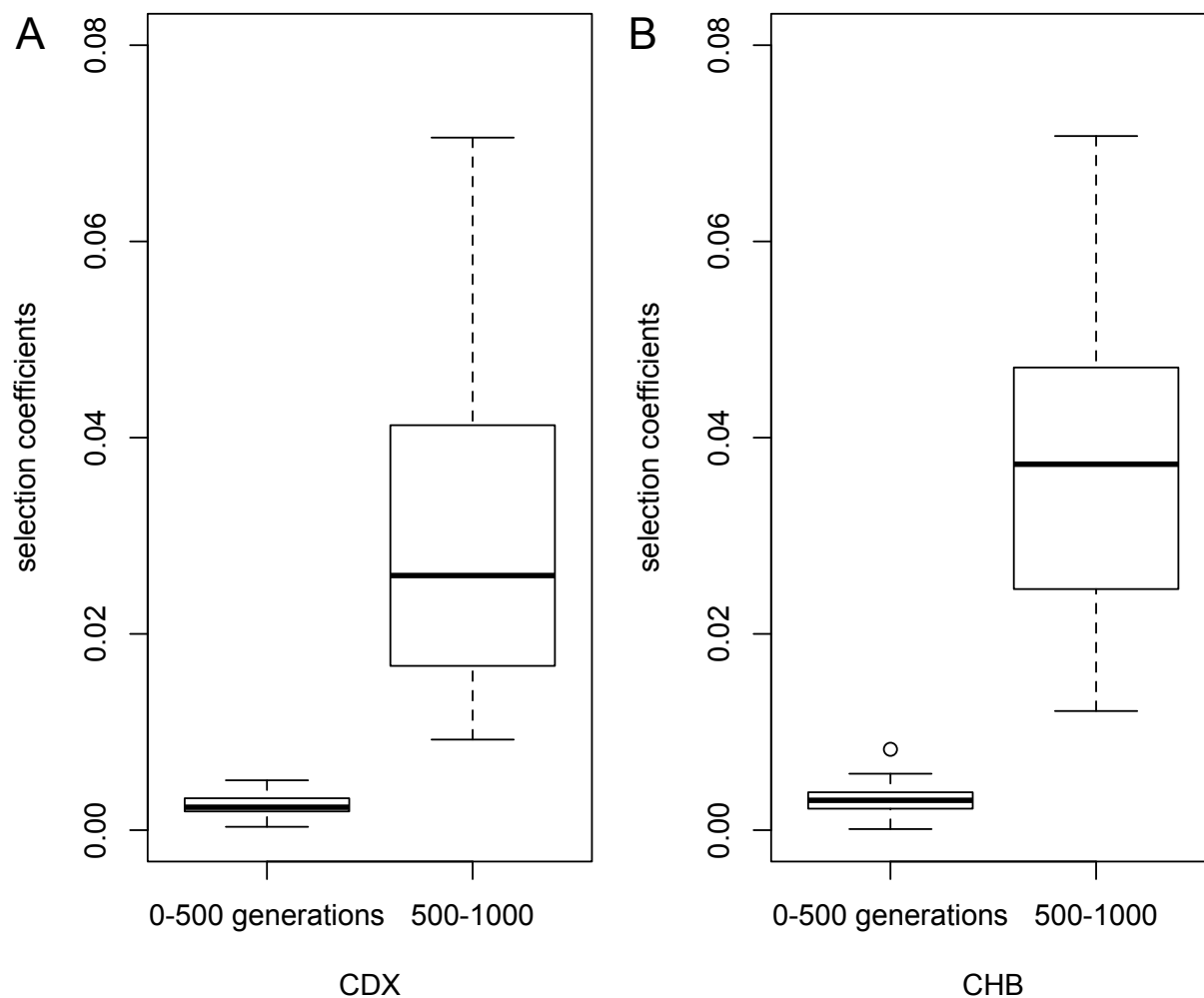
Figure 5. Coronavirus selected VIPs selection coefficients estimated by CLUES
This figure shows classic R boxplots of selected coefficients at the 42 Relate selected mutations within the peak around 900 generations ago (Methods). A) Selection coefficients in the Chinese Dai CDX 1,000 Genomes population. B) Selection coefficients in the Han Chinese from Beijing CHB 1,000 Genomes population. Left: average selection coefficients between 0 and 500 generations ago. Right: average selection coefficients between 500 and 1,000 generations ago.

Selected CoV-VIPs are enriched for antiviral and proviral factors

To further clarify that an ancient viral epidemic caused the strong burst of selection we observe in the ancestors of East Asians, and not another ecological pressure acting on the same set of genes, we test if the 42 selected CoV-VIPs are enriched for genes with antiviral or proviral effects relative to other CoV-VIPs (i.e. loci that are known to have a detrimental or beneficial effect on the virus, respectively). Because the relevant literature for coronaviruses is currently limited – which also applies to the relatively recent SARS-CoV-2 virus – we extend our set of

15

359   anti- and proviral loci beyond those associated with coronaviruses to include loci reported for

360   diverse viruses with high confidence from the general virology literature (see SI: *Host adaptation*

361   *is expected at VIPs*; Table S1). We find that 21 (50%) of the 42 CoV-VIPs that came under

362   selection ~900 generations ago have high-confidence anti- or proviral effects (vs. 29% for all

363   420 CoV-VIPs), a significant inflation in anti- and proviral effects (hypergeometric test P=6.10^{-4})

364   that further supports our claim that the underlying selective pressure was most likely a viral

365   epidemic. This overlap of antiviral and proviral effects between different viruses also implies that

366   an unknown virus that happened to use similar VIPs as coronaviruses could have indeed been

367   responsible.

Selected mutations lie near regulatory variants active in SARS-CoV-2 affected tissues

369   Coronavirus infections in humans are known to have pathological consequences for specific

370   bodily tissues, whereby we investigate if the genes targeted by selection in the ancestors of

371   East Asians are also enriched for regulatory functions in similar tissues. In light of our finding

372   that many putative causal mutations in CoV-VIPs were proximal to eQTLs, we investigate

373   whether selected mutations are situated closer to eQTLs for a given tissue than expected by

374   chance, as this would indicate that the tissue was negatively impacted by the virus (prompting

375   the adaptive response). Note that the GTEx eQTLs we use are not specific to a single tissue

376   (eQTLs are rarely so in general), and are shared between tissues. However, each tissue still

377   has its own specific combination of eQTLs, thus making the results at each tissue not

378   completely redundant. Briefly, we estimate a proximity-based metric that quantifies the distance

379   between the location of the causal mutation estimated by iSAFE and the tissue-specific eQTLs

380   for the 42 loci that likely started coming under selection ~900 generations ago, and compare

381   this to the same distances observed amongst randomly sampled sets of CoV-VIPs (Figure 6;

382   Methods).

383   Using this approach, we find that GTEx lung eQTLs lie closer to predicted causal mutations

384   amongst the 42 putative selected loci than for any other tissue (P=3.10^{-5}; Figure 6). Several

385   additional tissues known to be negatively affected by coronavirus – blood and arteries (Bao et

386   al., 2020; Grosse et al., 2020), adipose tissue (Michalakis and Ilias, 2020) and the digestive

387   tract (Elmunzer et al., 2020) – also exhibit closer proximities between putative causal loci and

388   tissue-specific eQTLs than expected by chance (Figure 6). Interestingly, the spleen shows no

389   tendency for eQTLs to lie closer to selected loci than expected around 900 generations ago

390   compared to other evolutionary times, perhaps because the spleen is replete with multiple types

16

391   of immune cells that might be more prone to more regular adaptation in response to diverse

392   pathogens over time, and less prone to adaptive bursts restricted over time in response to a

393   specific pathogen (Quintana-Murci, 2019). Note that tissues with more eQTLs tend to have

394   more significant p-values. For example skeletal muscle has a lower proximity ratio than stomach

395   but also a lower p-value due to the higher statistical power provided by more eQTLs. Our results

396   indicate that the tissues impacted in the inferred viral epidemic in ancestors of East Asians

397   match those pathologically affected by the SARS-CoV-2 infection in contemporary populations,

398   providing further evidence that this ancient infection might have been a coronavirus or another

399   type of virus that used similar host interactions.

400
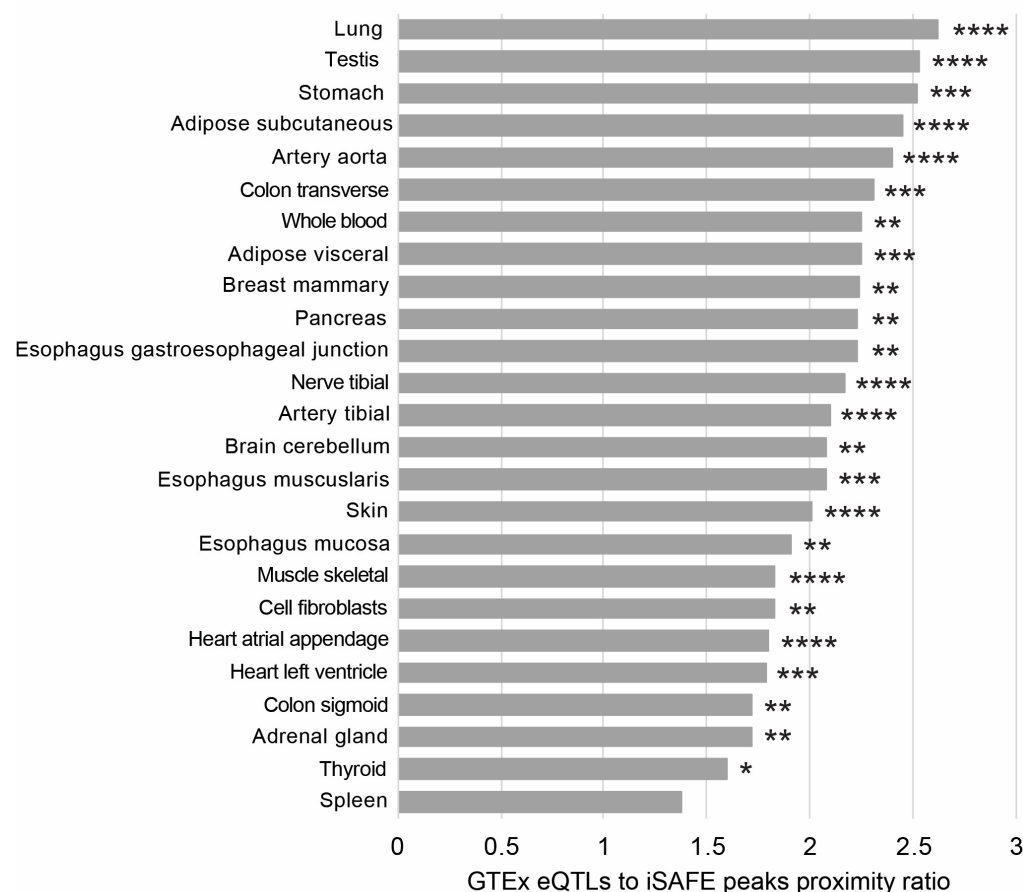
Figure 6. Proximity of selection signals to GTEx eQTLs at the 42 selected CoV-VIPs compared to random CoV-VIPs

403   The histogram shows how close selection signals localized by iSAFE peaks are to the GTEx

404   eQTLs from 25 different tissues, at peak-VIPs compared to randomly chosen CoV-VIPs

405   (Methods). How close iSAFE peaks are to GTEx eQTLs compared to random CoV-VIPs is

406   estimated through a proximity ratio. The proximity ratio is described in the Methods. It quantifies

407   how much closer iSAFE peaks are to eQTLs of a specific GTEx tissue, compared to random

17

408   expectations that take the number and structure of iSAFE peaks, as well as the number and

409   structure of GTEx eQTLs into account (Methods). Four stars: proximity ratio test P<0.0001.

410   Three stars: proximity ratio test P<0.001. Two stars: P<0.01. One star: P<0.05. Note that lower

411   proximity ratios can be associated with smaller p-values for tissues with more eQTLs (due to

412   decreased null variance; for example, skeletal muscle vs. pancreas).

Coronavirus VIPs are enriched for SARS-CoV-2 susceptibility and COVID-19 severity loci

414   Our results indicate that many of the selected CoV-VIPs now sit at intermediate to high

415   frequencies in modern East Asian populations. Accordingly, we anticipate that these

416   segregating loci should make a measurable contribution to the inter-individual variation in

417   SARS-CoV-2 susceptibility and (COVID-19) severity amongst contemporary populations in East

418   Asia, and predict that such loci would be readily detectable in a reasonably-powered genome

419   wide association study (GWAS) investigating these traits in East Asian populations. While such

420   a scan has yet to be reported for a large East Asian cohort, two GWASs were recently released

421   that used sizable British cohorts to investigate SARS-CoV-2 susceptibility (1,454 cases and

422   7,032 controls; henceforth called the susceptibility GWAS) and severity (325 cases [deaths]

423   versus 1,129 positive controls; henceforth called the severity GWAS) (data from the UK

424   Biobank; Sudlow et al., 2015; https://grasp.nhlbi.nih.gov/Covid19GWASResults.aspx). Because

425   we use a different population than the ones where we found selection, we only ask, as a form of

426   functional validation of a viral pressure, if there is an overlap between the selected loci in East

427   Asia and stronger COVID-19 GWAS hits in the UK Biobank cohort. We do not look at all at the

428   directionality or the size of effects, as it is dubious that those would be transposable between

429   populations. This also means that we make no claim at all here about any decrease or increase

430   of virus susceptibility in any given human population compared to others. Furthermore, we use

431   the UK-Biobank cohort instead of the complete COVID-19 Host Genetics Initiative meta-GWAS

432   data (https://www.covid19hg.org/; The COVID-19 Host Genetics Initiative, 2020), to avoid

433   population stratification to the best extent possible (a legitimate concern with a trait clearly

434   affected by environmental factors).

435   While we are unable to precisely identify the causal variants for the selected CoV-VIP genes

436   observed in the ancestors of East Asians – nor would these variants necessarily occur as

437   outliers in a GWAS conducted on the British population – we note that it is possible that other

438   variants in the same CoV-VIP genes may also produce variation in SARS-CoV-2 susceptibility

439   and severity amongst modern British individuals.

440   By contrasting variants in CoV-VIPs against those in random sets of genes, we find that variants

441   in CoV-VIPs have significantly lower p-values for both the susceptibility GWAS and severity

442   GWAS than expected (simple permutation test $P<10^{-9}$ for both GWAS tests; Methods). More

443   importantly, the 42 CoV-VIPs from the selection event starting ~900 generations ago have even

444   lower GWAS p-values compared to other CoV-VIPs (P=0.0015 for susceptibility GWAS and

445   P=0.023 for severity GWAS; Methods). This result indicates that the selected genes inferred in

446   our study might contribute to individual variation in COVID-19 etiology in modern human

447   populations in the UK, providing further evidence that a coronavirus or another virus with similar

448   host interactions may have been the selection pressure behind the adaptive response we

449   observe in the ancestors of East Asians. Notably, the strongest GWAS hits identified by the

450   COVID-19 Host Genetics Initiative (listed at https://www.covid19hg.org/publications/) do not

451   overlap with the 42 CoV-VIPs selected in East Asia. We note however that we do not

452   necessarily expect the strongest GWAS hits in Europe to be strong hits in other populations. In

453   addition, although adaptation implies a functional genetic effect, a genetic effect does not

454   necessarily mean it has adaptive potential. The lack of overlap with the strongest COVID-19

455   Host Genetics Initiative hits is therefore not necessarily very surprising. It also does not take

456   away the fact that we found an enrichment in stronger GWAS hits on average at CoV-VIPs and

457   especially at selected CoV-VIPs.

458   **Selected CoV-VIP genes include multiple known drug targets**

459   Our analyses suggest that the 42 CoV-VIPs identified as putative targets of an ancient

460   coronavirus (or another virus using similar host interactions) epidemic might play a functional

461   role in SARS-CoV-2 etiology in modern human populations. We find that four of these genes

462   (*SMAD3*, *IMPDH2*, *PPIB*, *GPX1*) are targets of eleven drugs being currently used or

463   investigated in clinical trials to mitigate COVID-19 symptoms (Methods). While this number is

464   not higher than expected when compared to other CoV-VIPs (hypergeometric test P>0.05), we

465   note that most of the 42 genes identified here have yet to be the focus of clinical trials for SARS-

466   CoV-2-related drugs. In addition to the four selected CoV-VIP genes targeted by coronavirus-

467   specific drugs, five additional selected CoV-VIPs are targeted by multiple drugs to treat a variety

468   of non-coronavirus pathologies (Table S7). This raises the possibility that such drugs could be

469   repurposed for therapeutic use in the current SARS-CoV-2 pandemic. Indeed, an additional six

470   of the 42 selected CoV-VIPs have been identified by (Finan et al., 2017) as part of the

471   "druggable genome" (Table S7).

Discussion

By scanning 26 diverse human populations from five continental regions for evidence of strong selection acting on genes that interact with coronavirus strains (CoV-VIPs), we identified a set of 42 CoV-VIPs exhibiting a coordinated adaptive response that likely emerged more than 20,000 years ago (Figure 2). This pattern was unique to the ancestors of East Asian populations (as classified by the 1,000 Genomes, including South East Asia with the Kinh in Vietnam), being absent from any of the 21 non East-Asian human populations tested here. By using ARG methods to reconstruct the trajectories of selected alleles, we show that this selection pressure produced a strong response across the 42 CoV-VIP genes that gradually waned and resulted in the selected loci plateauing at intermediate frequencies. Further, we demonstrate that this adaptive response is likely the outcome of a multigenerational viral epidemic, as attested by the clustering of putatively selected loci around variants that regulate tissues known to exhibit COVID-19-related pathologies, and the enrichment of variants associated with SARS-CoV-2 susceptibility and severity, as well as anti- and proviral functions, amongst the 42 CoV-VIP genes selected starting around 900 generations ago.

An important limitation of our study is that some of our analyses rely upon comparative datasets that were generated in contemporary human populations that have different ancestries than the East Asian populations where the selected CoV-VIP genes were detected. In particular, both of the eQTL and GWAS datasets come from large studies that are primarily focused on contemporary populations from Europe, and none of the five European populations in our study exhibit the selection signals observed in the genomes of East Asians. Accordingly, more direct confirmation of the causal role of 42 CoV-VIP genes in COVID-19 etiology will require the appropriate GWAS to be conducted in East Asian populations. The detection of genetic associations amongst the 42 CoV-VIPs in a GWAS on contemporary East Asians would provide further evidence that one or more coronaviruses, or another virus using similar interactions, comprised the selection pressure that drove the observed adaptive response. Moreover, a high-powered GWAS in East Asian populations would be required to identify the loci that currently impact individual variation in COVID-19 etiology in East Asian individuals. Because of these limitations, and because it would be extremely difficult to control for all the other factors that differ across the world (including socioeconomic factors), our results do not represent evidence for any difference in either increased or decreased genetic susceptibility in any human population.

20

Insights into ancient viral epidemics from modern human genomes

504   A particularly salient feature of the adaptive response observed for the 42 CoV-VIPs is that
505   selection appears to be acting continuously over a ~20,000 years period, with the caveat that
506   the start of selection is complex to pinpoint as shown by the analysis of the selected alleles
507   frequency trajectories (Figure 3). The activity of a viral pressure over such an extensive time
508   period is not consistent with epidemics that started in recorded human history, which tend to be
509   circumscribed to a few generations. A possible hypothesis is that the viral pressure remained
510   present throughout the 20,000 year period, but was only initially strong enough to qualify as a
511   full-blown pandemic in the commonly understood sense, before becoming less severe over time
512   as a consequence of host adaptation and/or a reduction in virulence. As this manuscript was in
513   the final stages of preparation, the first host-virus interactomes were published for SARS-CoV-1
514   and MERS-CoV, which exhibit an extensive overlap with the SARS-CoV-2 interactome used in
515   the present study (Gordon et al., 2020). This suggests that coronaviruses share a broad set of
516   host proteins that they interact with, which should also apply to ancient coronaviruses. These
517   patterns are consistent with one or more coronaviruses driving selection events in East Asian
518   prehistory that produced the signals that we report here. That said, and as already mentioned,
519   we cannot exclude that another, currently unknown type of viruses might have been
520   responsible, that used the same interactions as coronaviruses with human proteins. The
521   cumulated evidence in this study still clearly points towards an ancient viral selective pressure.

522   Further validation of the historical trajectories of the causal mutations at selected genes is still
523   needed, including more finely resolved temporal and geographic patterns that could be derived
524   from ancient DNA sampled from across East Asia that span the human occupation of this
525   region; however, the requisite ancient samples are lacking at the moment. Nonetheless, we
526   note the geographic origin of several modern outbreaks of coronaviruses in East Asia, point to
527   East Asia being a likely location where these ancient populations came into contact with the
528   virus. Given that multiple recently recorded coronavirus outbreaks have been traced to
529   zoonoses (direct or indirect with other animal intermediates) from East Asian bats (Wong et al.,
530   2019), our results suggest that East Asia might have also been a natural range for coronavirus
531   reservoir species during the last 25,000 years.

Applied evolutionary medicine: using evolutionary information to combat COVID-19

534   The net result of the ancient selection patterns on the CoV-VIPs in ancient human populations is
535   the creation of genetic differences amongst individuals now living in East Asia, and between

536   East Asians and populations distributed across the rest of the world. As we demonstrate in this

537   study, this evolutionary genetic information can be exploited by statistical analyses to identify

538   loci that are potentially involved in the epidemiology of modern diseases – COVID-19 in the

539   present case. Such evolutionary information may ultimately assist in the development of future

540   drugs and therapies, by complementing information obtained from more traditional

541   epidemiological and biomedical research. For example, a recent study focusing on *TMPRSS2* –

542   a gene encoding for a transmembrane protein that plays a key role in SARS-CoV-2 infection –

543   found that East Asian populations carry two protein coding variant that are correlated with low

544   fatality rate for COVID-19 cases (Jeon et al., 2020). While such studies provide high quality

545   information on a specific gene, the evolutionary approach adopted here is able to leverage

546   evolutionary information embedded in modern genomes to identify candidate genomic regions

547   of interest. This is similar to the information provided by GWAS – i.e. lists of variants or genes

548   that are potentially associated with a particular trait or disease – though we note that the

549   information provided by evolutionary analyses comes with an added understanding about the

550   historical processes that created the underlying population genetic patterns.

551   The current limitation shared by population genomic approaches such as GWAS and the

552   evolutionary analyses presented here, is that they identify statistical associations, rather than

553   causal links, between genomic regions and traits, thereby necessitating additional research to

554   confirm causality. In addition to the various forms of empirical information that we provide here,

555   further evidence of causal relationships between the CoV-VIPs and COVID-19 etiology could be

556   obtained by examining which viral proteins the selected CoV-VIPs interact with, thus

557   establishing the specific viral functions that are affected. As a preliminary observation, we find

558   that the 35 of the 42 selected SARS-CoV-2 VIPs tend to interact with more viral proteins than

559   expected by chance (13 instead of six expected, see SI). Such information will help establish

560   genetic causality and will also improve our understanding of how hosts adapt in response to

561   viruses.

562   The ultimate confirmation of causality requires functional validation that the genes interact with

563   the virus, or that drugs targeting these genes have a knock-on impact for the virus. Notably,

564   several CoV-VIP genes are existing drug targets showing the functional importance of these

565   particular loci (Table S7), several of which are currently being investigated or used to treat

566   severe cases in the current COVID-19 pandemic. It remains to be established if the other genes

567   we have identified in this study might also help guide drug repurposing efforts and provide a

568   basis for future drug and therapeutic development to combat COVID-19 and related

569 pathologies. It also remains to be established if population-specific past adaptation, and the
570 underlying selected changes at those genes, could imply different drug efficacies in different
571 human populations.

572 ## Conclusion

573 By leveraging the evolutionary information contained in publicly available human genomic
574 datasets, we were able to infer ancient viral epidemics impacting the ancestors of contemporary
575 East Asian populations, which initially arose likely more than 20,000 years ago, resulting in
576 coordinated adaptive changes across 42 genes. Importantly, our evolutionary genomic analyses
577 have identified several new candidate genes that might benefit current efforts to combat COVID-
578 19, either by providing novel drug targets or by repurposing currently available drugs that target
579 these candidate genes (Tables S4 & S6). More broadly, our findings highlight the utility of
580 thinking about the possible contribution of evolutionary genomic approaches into standard
581 medical research protocols. Indeed, by revealing the identity of our ancient pathogenic foes,
582 evolutionary genomic methods may ultimately improve our ability to predict – and thus prevent –
583 the epidemics of the future.

584

585

586

587
588

Methods

Important note: for convenience, the 42 CoV-VIPs that we infer to have started coming under selection around 900 generations ago are called peak-VIPs in the Methods.

Key resources table

REAGENT or RESOURCE	SOURCE	IDENTIFIER
Deposited Data		
1000 Genome Project - Phase 3	(1000 Genomes Project Consortium, 2015)	ftp://ftp.1000genomes.ebi.ac.uk/vol1/ftp/release/20130502/
VIPs	–this manuscript	–Table S1
Relate-estimated coalescence rates, allele ages and selection P-values for the 1000GP	(Speidel et al., 2019)	https://zenodo.org/record/3234689
GTEx expression	(GTEx Project, 2017)	https://gtexportal.org/home/datasets
Protein-protein interactions (IntAct)	(Luisi et al., 2015)	https://www.ebi.ac.uk/intact
The density of conserved segments (PhastCons)	(Siepel et al., 2005)	http://hgdownload.cse.ucsc.edu/goldenPath/hg19/phastCons46way/
The density of regulatory elements	–	http://hgdownload.soe.ucsc.edu/goldenPath/hg19/encodeDCC/wgEncodeRegDnaseClustered
The recombination rate	(Hinch et al., 2011)	https://www.well.ox.ac.uk/~anjali/AAmap/
Software and Algorithms		

24

selscan (compute nSL).	(Szpiech and Hernandez, 2014)	https://github.com/szpiech/selscan
hapbin (compute iHS)	(Maclean et al., 2015)	https://github.com/evotools/hapbin
Gene Set Enrichment Pipeline	(Enard and Petrov, 2020)	https://github.com/DavidPierreEnard/Gene_Set_Enrichment_Pipeline
Relate	(Speidel et al., 2019)	https://myersgroup.github.io/relate/
CLUES	(Stern et al., 2019)	https://github.com/35ajstern/clues
iSAFE	(Akbari et al., 2018)	https://github.com/alek0991/iSAFE

594

Coronavirus VIPs

596 We used a dataset of 5,291 VIPs (Table S1). Of these, 1,920 of these VIPs are high confidence

597 VIPs identified by low-throughput molecular methods, while the remaining VIPs were identified

598 by diverse high-throughput mass-spectrometry studies. For a more detailed description of the

599 VIPs dataset, please refer to SI: Host adaptation is expected at VIPs.

Genomes and sweeps summary statistics

601 To detect signatures of adaptation in various human populations, we used the 1,000 Genome

602 Project phase 3 dataset which provides chromosome level phased data for 26 distinct human

603 populations representing all major continental groups (1000 Genomes Project Consortium,

604 2015). To measure nSL separately in each of the 26 populations, we used the selscan software

605 available at https://github.com/szpiech/selscan (Szpiech and Hernandez, 2014). To measure

606 iHS, we used the hapbin software available at https://github.com/evotools/hapbin (Maclean et

607 al., 2015).

Ranking of sweep signals at protein-coding genes and varying window sizes

608 To detect sweep enrichments at CoV-VIPs, we first order, separately in each of the 26 1,000

609 Genomes populations, human Ensembl (Cunningham et al., 2019) (version 83) protein-coding

611 genes according to the intensity of the sweep signals at each gene. As a proxy for the intensity

612 of these signals, we use the average of either iHS or nSL across all the SNPs with iHS or nSL

613 values within a window of fixed size, centered at the genomic center of genes, halfway between

614 the most upstream transcription start site and the most downstream transcription end site. We

615 then rank the genes according to the average iHS or nSL (more precisely their absolute values)

616 in these windows. We get six rankings for six different fixed window sizes: 50kb, 100kb, 200kb,

617 500kb, 1,000kb and 2,000kb. We do this to account for the variable size of sweeps of different

618 strengths. We then estimate the sweep enrichment at CoV-VIPs compared to controls over all

619 these different window sizes considered together, or at specific sizes, as described below and in

620 Enard & Petrov (Enard and Petrov, 2020).

Estimating the whole ranking curve enrichment at CoV-VIPs and its statistical significance

623 To estimate a sweep enrichment in a set of genes, a typical approach is to use the outlier

624 approach to select, for example, the top 1% of genes with the most extreme signals. Here we

625 use a previously described approach to estimate a sweep enrichment while relaxing the

626 requirement to identify a single top set of genes. Instead of, for example, only estimating an

627 enrichment in the top 100 genes with the strongest sweep signals, we estimate the enrichment

628 over a wide range of top X genes, where X is allowed to vary from the top 10,000 to the top 10

629 with many intermediate values. This creates an enrichment curve as in Figure 1. Figure 1 shows

630 the estimated relative fold enrichments at CoV-VIPs compared to controls, from the top 1,000 to

631 the top 10 nSL. The statistical significance of the whole enrichment curve can then be estimated

632 by using block-randomized genomes, as described in Enard & Petrov (Enard and Petrov, 2020).

633 In brief, block-randomized genomes make it possible to generate a large number of random

634 whole enrichment curves while maintaining the same level of clustering of genes in the same

635 candidate sweeps as in the real genome, which effectively controls for gene clustering.

636 Comparing the real whole enrichment curve to the random ones then makes it possible to

637 estimate an unbiased false-positive risk (also known as False Discovery Rate in the context of

638 multiple testing) for the observed whole enrichment curve at CoV-VIPs. A single false positive

639 risk can be estimated for not just one curve but by summing over multiple curves combined,

640 thus making it possible to estimate a single false positive risk over any arbitrary numbers of rank

26

641   thresholds, window sizes, summary statistics, and populations. For instance, we estimate the

642   false-positive enrichment risk of P=2.10^{-4} at CoV-VIPs for rank threshold from the top 10,000 to

643   top 10, over six window sizes, for the five East Asian populations in the 1,000 Genomes data,

644   and for both nSL and iHS, all considered together at once. This makes our approach more

645   versatile and sensitive to selection signals ranging from a few very strong sweeps, to many,

646   more moderately polygenic hitchhiking signals. The entire pipeline to estimate false-positive

647   risks with block-randomized genomes is available at

648   https://github.com/DavidPierreEnard/Gene_Set_Enrichment_Pipeline (Enard and Petrov, 2020).

649   **Building sets of controls matching for confounding factors**

650   To estimate a sweep enrichment at CoV-VIPs, we compare CoV-VIPs with random control sets

651   of genes selected far enough (>500kb) from CoV-VIPs that they are unlikely to overlap the

652   same large sweeps. We do not compare CoV-VIPs with completely random sets of control

653   genes. Instead, we use a previously described bootstrap test to build random control sets of

654   genes that match CoV-VIPs for a number of potential confounding factors that might explain a

655   sweep enrichment, rather than interactions with viruses. The bootstrap test has been described

656   in detail (Enard and Petrov, 2020), and is available at

657   https://github.com/DavidPierreEnard/Gene_Set_Enrichment_Pipeline.

658   We include 11 different potential confounding factors in the bootstrap test:

659   - average GTEx expression in 53 GTEx V6 tissues.

660   - GTEx expression in lymphocytes.

661   - GTEx expression in testis.

662   - the number of protein-protein interactions from the Intact database, curated by Luisi et al.

663   (Luisi et al., 2015).

664   - the Ensembl (v83) coding sequence density in a 50kb window centered on each gene.

665   - the density of conserved segments identified by PhastCons (Siepel et al., 2005)

666   (http://hgdownload.cse.ucsc.edu/goldenPath/hg19/phastCons46way/).

667   - the density of regulatory elements, estimated by the density of Encode DNase I V3 Clusters

668   (http://hgdownload.soe.ucsc.edu/goldenPath/hg19/encodeDCC/wgEncodeRegDnaseClustered/)

669   in a 50kb window centered on each gene.

670   - the recombination rate in a 200kb window centered on each gene (Hinch et al., 2011).

671   - the GC content in a 50kb window centered on each gene.

672   - the number of bacteria each gene interacts with, according to the Intact database (as of June

673   2019; https://www.ebi.ac.uk/intact/).

674   - the proportion of genes that are immune genes according to Gene Ontology annotations

675   GO:0006952 (defense response), GO:0006955 (immune response), and GO:0002376 (immune

676   system process) as of May 2020.

677   **Estimating adaptation start times at specific genes with Relate**

678   As times of emergence of adaptive mutations, we use the publicly available estimates from

679   Relate (https://myersgroup.github.io/relate/). Relate estimates mutation emergence times while

680   controlling for fluctuations of population size over time, based on the coalescence rates it

681   reconstructs after inferring ancestral recombination graphs at the scale of the whole genome

682   (Speidel et al., 2019). Relate provides two times of emergence of mutations, one low estimate

683   (less generations ago), and one high estimate (more generations ago). The low time estimate

684   corresponds to the time when Relate estimates an elevated probability that the frequency of the

685   mutation is different from zero. The high time estimate corresponds to the time when Relate

686   estimates that the probability is not too small that the frequency of the mutation is different from

687   zero. For our purpose of estimating when selection started, the low time estimate is the best

688   suited, because it provides an estimate of when the frequency of a selected mutation was

689   already high enough to distinguish from zero, for those mutations where selection started from a

690   very low frequency. For cases where selection started with standing genetic variants that were

691   already distinguishable from zero, the Relate low time estimates for the emergence of mutations

692   do not provide a good proxy for when selection actually started. Thus, if we were able to

693   estimate when selection started for standing genetic variants, we might be able to observe an

694   even stronger peak than the one we see when just relying on those variants where selection

695   started from low frequencies.

696   Using the low Relate time estimates is also justified due to the fact that the sweep establishment

697   phase can take very variable amounts of time before the start of the sweep exponential phase.

698   During the establishment phase, selected alleles are still mostly governed by drift which makes

699   pinpointing the actual starting time of selection difficult. In this context, the low Relate time

700   estimates provide an estimate of the time when the selected alleles were no longer at very low

701   frequencies not statistically different from zero, and closer to entering the exponential phase,

702   which provides a more certain time estimate for when selection started for certain.

703   An important step is then to choose at each CoV-VIP locus, and all the other control loci, which

704   Relate mutation to use to get a single time estimate for each locus. Note that here we make an

705   assumption that each locus has experienced only one single adaptive event. Given our finding

706   that iSAFE peaks at CoV-VIPs are much closer to GTEx V8 eQTLs than expected by chance, it

707   is likely that the selected adaptive mutations are regulatory mutations at, or close to annotated

708   eQTLs for a specific gene. They are not necessarily exactly located at eQTLs, because current

709   eQTLs annotations may still be incomplete, and in our case we use eQTLs identified in GTEx

710   V8 using mostly European individuals, even though we analyse selection signals in East Asian

711   populations. Because of these limitations, we use the Relate estimated time at the mutation

712   where Relate estimates the lowest positive selection p-value within 50kb windows centered on

713   eQTLs. We also only consider variants with a minor allele frequency greater than 20%, given

714   the signals detected by iHS and nSL that only have some power to detect incomplete sweeps

715   above 20% frequencies (Ferrer-Admetlla et al., 2014; Voight et al., 2006). This also excludes a

716   potential risk of confounding by low frequency neutral or weakly deleterious variants, that can

717   show selection-like patterns when their only way to escape removal early on is through a

718   chance, rapid frequency increase that can look like selection. The Relate selection test is based

719   on faster than expected coalescence rates given the population size at any given time, and its

720   results are publicly available at https://myersgroup.github.io/relate/. Note that the mutation with

721   the lowest Relate p-value does not always overlap with an iSAFE peak (Figure S5), which is not

722   entirely surprising if the haplotype signals exploited by both Relate and iSAFE partly

723   deteriorated due to recombination since the time selection at CoV-VIPs was strong (Figures 3

724   and 5). Both of these methods are indeed designed to locate the selected variant right after, or

725   during, active selection.

726   Because we work with five different East Asian populations, we more specifically select the

727   variant with the lowest Relate selection test p-value on average across all the five East Asian

728   populations. Then, we also use the corresponding average low Relate mutation time estimate

729   across the five East Asian populations. We do not attempt to estimate the selection time and p-

730   value by considering all 1,000 Genomes East Asian individuals tested together by Relate,

731   because then the Relate selection test is at a greater risk of being confounded by population

732   structure. Finally, we only consider CoV-VIPs and other control genes with an average Relate

733   selection test p-value lower than 10^{-3}, to make sure that we indeed use estimated times at

734   selected variants.

29

The peak significance test

736 To test if the peak of Relate time estimates around 900 generations ago at CoV-VIPs (Figure 2)

737 is expected simply by chance or not, we designed a peak significance test. The test compares

738 the peak at CoV-VIPs, with the top peaks obtained when repeatedly randomly sampling sets of

739 genes. We first identify the most prominent peak at CoV-VIPs by visual inspection of the pink

740 distribution of Relate times for CoV-VIPs compared to the blue distribution of Relate times for all

741 protein-coding genes with an estimated Relate time (Figure 2). To build these distributions, top

742 Relate selected mutations shared between multiple neighboring genes (CoV-VIPs or controls)

743 are counted only once, to avoid a confounding effect of gene clustering (152 selected variants at

744 CoV-VIPs, 1771 selected variants for all protein coding genes). The peak around 900

745 generations ago (870 generations more exactly) spans approximately 200 generations, where

746 the pink distribution is clearly above the blue one. We then use a 200 generations-wide window,

747 sliding every generation from 0 to 6,000 generations to verify the peak more rigorously. Sliding

748 one generation after another, each time we count the difference between the number of Relate

749 selected variants at CoV-VIPs that fall in the sliding 200 generations window, and the number of

750 Relate selected variants at all other genes that are not CoV-VIPs, weighted by the percentage

751 of variants found at CoV-VIPs, to correct for the different size of the two sets of variants. Using

752 this sliding window approach, the top of the peak is found at 870 generations, with a difference

753 of 19.5 additional Relate selected variants between 770 and 970 (870 plus or minus 100) at

754 CoV-VIPs compared to the null expectation.

755 We then repeat the sliding of a 200 generations window to identify the maximum peak and

756 measure the same difference, but this time for random sets of Relate selected variants of the

757 same size (152 selected variants out of the 1,771 selected variants). To estimate p-values, we

758 then compare the actual observed difference with the distribution of differences generated with

759 one million random samples.

760 As mentioned in the Results, one potential issue is that we run the peak significance test after

761 we already know that CoV-VIPs are enriched for iHS and nSL top sweeps, and especially

762 enriched for nSL top sweeps. This enrichment may skew the null expectation for the distribution

763 of Relate times at CoV-VIPs. In other words, there is a risk that any set of genes with the same

764 sweep enrichment might exhibit the same peak as CoV-VIP. As a result, comparing CoV-VIPs

765 with randomly chosen non-CoV-VIPs may not be appropriate. To test this, we repeat the peak

766 significance test, but this time comparing the peak at CoV-VIPs with the peaks at random sets

767 of non-CoV-VIPs that we build to have the same distribution of nSL ranks as CoV-VIPs. To do

30

768   this, we define nSL bins between ranks 1 and the highest rank with a rank step of 100 between

769   each bin, and we count how many Relate selected variants fall in each bin (each gene has one

770   nSL rank and one Relate selected variant). To build the random set, we then fill each of the 100

771   bins with the same number of random non-CoV-VIPs, as long as their nSL rank falls within that

772   bin. We use the average nSL rank over the five East Asian populations, and the lower

773   population-averaged rank of either 1 Mb or 2Mb window sizes (where we observe the strongest

774   enrichment at CoV-VIPs, see Results). The results of the peak significance test are unchanged

775   when using the matching nSL distribution (peak significance test P=1.10-4 vs. P=2.3.10-4

776   without matching nSL distribution).

777   In further agreement with the fact that the sweep enrichment does not confound the peak

778   significance test, the peak at CoV-VIPs stands out more when repeating the peak significance

779   test using a smaller nSL top rank limit (Figure S6). In this case, we compare sets of CoV-VIPs

780   and sets of controls both enriched in stronger sweep signals. Thus, if stronger sweep signals at

781   CoV-VIPs biased the peak significance test, we would expect the peak to fade away when

782   comparing only CoV-VIPs and controls both with stronger nSL signals. Conversely, we observe

783   that half of the CoV-VIPs with the weaker nSL signals (population-averaged nSL rank higher

784   than 7,200 for both 1Mb and 2Mb windows) do not show a significant peak (peak significance

785   test P=0.53).

786   **The iSAFE peaks/eQTL proximity test**

787   Adaptation in the human genome was likely mostly regulatory adaptation through gene

788   expression changes (Enard et al., 2014; Kudaravalli et al., 2009; Nédélec et al., 2016; Quach et

789   al., 2016). To test if positive selection at CoV-VIPs likely involved regulatory changes, we ask

790   whether the signals of adaptation around CoV-VIPs are localized closer than expected by

791   chance to GTEx eQTLs that affect the expression of CoV-VIPs in present human populations.

792   Indeed, the genomic regions at or close to CoV-VIP GTEx eQTLs are likely enriched for CoV-

793   VIP regulatory elements, and therefore the most likely place to find CoV-VIP-related adaptations

794   in the genome. To localize where adaptation occurred, we use the iSAFE method that was

795   specifically designed for this purpose (Akbari et al., 2018). iSAFE scans the genome and

796   estimates a score that increases together with proximity to the actual selected mutation. The

797   higher the score, the higher the odds that the scored variant is itself the selected one, or close

798   to the selected one. An important caveat is that iSAFE is designed to localize where selection

799   happened right after it happened, or as selection is still ongoing. In our case, we have evidence

800   that selection was strong at CoV-VIPs only more than 500 generations (~14,000 years) ago,

801   and then much weaker more recently (Figure 5). This could be an issue, because we expect

802   that recombination events that occurred after the strong selection might have deteriorated the

803   iSAFE signal that relies on haplotype structure. This is because recombination mixes together

804   the haplotypes that hitchhiked with the selected mutation, with those that did not. In line with

805   this, we often do not observe simple, clean iSAFE score peaks, but instead, iSAFE score

806   plateaus and more rugged peaks (Figure S5). For this reason, we designed an approach to not

807   only identify the top of simple iSAFE peaks, but also more rugged peaks or plateaus. First, to

808   measure iSAFE scores, we combine all the haplotypes from the five East Asian populations

809   together as input, since we found that the selection signal at CoV-VIPs is common to all these

810   populations (iSAFE parameters: --IgnoreGaps --MaxRegionSize 250000000 --window 300 --

811   step 100 --MaxFreq .95 --MaxRank 15). We then use a 500kb window sliding every 10kb to

812   identify the highest local iSAFE value in the 500kb window (Figure S8). Once we have the

813   highest local iSAFE value and coordinate, we define a broader iSAFE peak as the region both

814   upstream and downstream where the iSAFE values are still within 80% of the maximum value

815   (Figure S8). This way, we can better annotate iSAFE plateaus and rugged peaks, and take into

816   account the fact that they can span more than just a narrow local maximum (Figure S5).

817   Once the local iSAFE peaks are identified, we can ask how close GTEx eQTLs are to these

818   peaks compared to random expectations. We first measure the distance of each CoV-VIP GTEx

819   eQTL to the closest iSAFE peak. To avoid redundancy, we merge eQTLs closer than 1kb to

820   each other into one test eQTL at the closest, lower multiple of 1,000 genomic coordinates (for

821   example 3,230 and 3,950 would both become 3,000). We then measure the average of the log

822   of the distance between all CoV-VIPs and their closest iSAFE peak. We use the log (base 10) of

823   the distance, because it matters if the eQTL/iSAFE peak distance is 100 bases instead of

824   200kb, but it does not really matter if the distance is 200kb or 600kb, because the iSAFE peak

825   at 300kb is likely not related to the eQTL more than the peak at 600kb. Once we have the

826   average of log-distances, we compare it to its random expected distribution. To get this random

827   distribution, we measure the log-distance between each CoV-VIP eQTL and the iSAFE peaks,

828   but after shifting the iSAFE scores left or right by a random value between 1Mb and 2Mb (Figure

829   S8; less, or no shift at all if this falls within telomeres or centromeres). We shift by at least 1Mb

830   to make sure that we do not rebuild the original overlap of iSAFE peaks with eQTLs again and

831   again (some iSAFE peaks, or more precisely rugged peaks and plateaus can be wide and

832   include several hundred kilobases; see Figure S5). The random shifting effectively breaks the

32

833   relationship between eQTLs and iSAFE peaks, while maintaining the same overall eQTL and

834   peak structure (and thus variance for the test). The random log-distance distribution then

835   provides an overall random average log-distance to compare the observed average long-

836   distance with, as well as estimate a p-value.

837   Then, to more specifically ask if lung eQTLs at CoV-VIPs or the eqTLs of other specific tissues

838   are closer to iSAFE peaks than expected by chance, we can do the same but only using the

839   eQTLs of that specific tissue. The analysis represented in figure 6 is however more complicated

840   than just testing if CoV-VIP eQTLs for a specific tissue are closer to iSAFE peaks than expected

841   by chance by randomly sliding iSAFE values. Instead, what we ask is whether the 42 peak-VIPs

842   have eQTLs for a given tissue that are even closer to iSAFE peaks than the eQTLs of all CoV-

843   VIPs in general. To test this, for example with lung eQTLs, we first estimate how close lung

844   eQTLs are to iSAFE peaks at peak-VIPs, compared to random expectations, by measuring the

845   difference between the observed and the average random log-distance, just as described

846   before. We then count the number of peak-VIPs with lung eQTLs (19 out of 25 peak-VIPs with

847   GTEx eQTLs), and we randomly select the same number of any CoV-VIP (which may randomly

848   include peak-VIPs) as long as the random set of CoV-VIPs has the same number of lung eQTLs

849   (plus or minus 10%) as the set of peak VIPs with lung eQTLs (the same gene can have multiple

850   eQTLs for one tissue). We make sure that the tested and the random sets have similar numbers

851   of genes and eQTLs so that the test has the appropriate null variance. We then measure the

852   difference between the observed log-distance, and the randomly expected average log-distance

853   for the random set of CoV-VIPs, exactly the same way we did before for the actual set of peak-

854   VIPs. We then measure the ratio of the observed difference in log-distance between peak-VIPs

855   and the random expectation after many random shiftings (1,000), divided by the average of the

856   same difference measured over many random sets of CoV-VIPs. The final ratio tells us how

857   much closer lung eQTLs are to iSAFE peaks at peak-VIPs compared to CoV-VIPs in general,

858   and still takes the specific eQTLs and iSAFE peak structures at each locus into account, since

859   we compare differences in log-distances expected while preserving the same eQTL and iSAFE

860   peak structure (see above the description of the random coordinate shifting). One important last

861   detail about the test is that because we already found that the 50% of loci with the lowest nSL

862   signals do not show a peak of selection at CoV-VIPs around 900 generations ago (see Results),

863   we do not use these loci in this test since any iSAFE peak there is much more likely to represent

864   random noise, not actual selection locations, and thus likely to dilute genuine signals. Using this

865   test, we find that lung and other tissues' eQTLs at peak-VIPs are much closer to iSAFE peaks

866   than they are at CoV-VIPs in general. This test thus specifically tells that adaptation happened

867   closer to lung eQTLs, specifically around 900 generations ago compared to other evolutionary

868   times. By estimating the same ratio for 24 other tissues with at least 10 peak-VIPs with the

869   specific tested tissue eQTLs, we can finally rank each tissue for its more pronounced

870   involvement in adaptation ~900 generations ago, as done in figure 6. It is particularly interesting

871   in this respect that the tissue with least evidence for being more involved in adaptation at that

872   time more than other evolutionary times is spleen. Spleen indeed likely represents a good

873   negative control as a tissue strongly enriched in immune cell types and likely to have evolved

874   adaptively for most of evolution.

875   **UK Biobank GWAS analysis**

876   To compare the UK Biobank GWAS p-values at different loci, we assigned one p-value for each

877   gene, either CoV-VIPs, peak-VIPs or other genes, even though each gene locus can have many

878   variants with associated GWAS p-values. To assign just one single GWAS p-value to each

879   gene, we selected the variant with the lowest p-value at or very close (<1kb) to GTEx eQTLs for

880   a specific gene, in line with the fact that GWAS hits tend to overlap eQTLs (Hormozdiari et al.,

881   2016), and to remain consistent with the rest of our manuscript. We then compared the average

882   p-value between different sets of genes using classic permutations (one billion iterations).

883   **Drug targets identification**

884   We queried the databases DGIdb (Cotto et al., 2017), and PanDrugs (Piñeiro-Yáñez et al.,

885   2018) for drugs targeting CoV-VIPs and peak-VIPs. For hits from PanDrugs we limited the

886   results to only genes that are in direct interaction with the designated drug. Drugs targeting

887   peak-VIPs are presented in Table S7. In addition, we present a list of peak-VIPs that are not

888   currently drug targets, but have been previously identified in (Finan et al., 2017) as viable drug

889   targets (druggable genome).

890   # Acknowledgments

894

895

Authors Contributions

Conceived and designed the experiments: YS, RT, DE. Performed the experiments: YS, MEL, RT, DE. Interpreted the results: YS, MEL, RT,CDH, ASJ, DE. Wrote the manuscript: YS, RT, DE

References

1000 Genomes Project Consortium (2015). A global reference for human genetic variation. Nature *526*, 68–74.

Akbari, A., Vitti, J.J., Iranmehr, A., Bakhtiari, M., Sabeti, P.C., Mirarab, S., and Bafna, V. (2018). Identifying the favored mutation in a positive selective sweep. Nat. Methods *15*, 279–282.

Balogun, O.D., Bea, V.J., and Phillips, E. (2020). Disparities in Cancer Outcomes Due to COVID-19—A Tale of 2 Cities. JAMA Oncol.

Bao, C., Tao, X., Cui, W., Yi, B., Pan, T., Young, K.H., and Qian, W. (2020). SARS-CoV-2 induced thrombocytopenia as an important biomarker significantly correlated with abnormal coagulation function, increased intravascular blood clot risk and mortality in COVID-19 patients. Exp. Hematol. Oncol. *9*, 16.

Barreiro, L.B., Ben-Ali, M., Quach, H., Laval, G., Patin, E., Pickrell, J.K., Bouchier, C., Tichit, M., Neyrolles, O., Gicquel, B., et al. (2009). Evolutionary dynamics of human Toll-like receptors and their different contributions to host defense. PLoS Genet. *5*, e1000562.

Best, S.M., and Kerr, P.J. (2000). Coevolution of host and virus: the pathogenesis of virulent and attenuated strains of myxoma virus in resistant and susceptible European rabbits. Virology *267*, 36–48.

Cotto, K.C., Wagner, A.H., Feng, Y.-Y., Kiwala, S., Coffman, A.C., Spies, G., Wollam, A., Spies, N.C., Griffith, O.L., and Griffith, M. (2017). DGIdb 3.0: a redesign and expansion of the drug–gene interaction database. Nucleic Acids Res. *46*, D1068–D1073.

Cunningham, F., Achuthan, P., Akanni, W., Allen, J., Amode, M.R., Armean, I.M., Bennett, R., Bhai, J., Billis, K., Boddu, S., et al. (2019). Ensembl 2019. Nucleic Acids Res. *47*, D745–D751.

Dong, E., Du, H., and Gardner, L. (2020). An interactive web-based dashboard to track COVID-19 in real time. Lancet Infect. Dis. *20*, 533–534.

eGTEx Project (2017). Enhancing GTEx by bridging the gaps between genotype, gene expression, and disease. Nat. Genet. *49*, 1664–1670.

Ellinghaus, D., Degenhardt, F., Bujanda, L., Buti, M., Albillos, A., Invernizzi, P., Fernández, J., Prati, D., Baselli, G., Asselta, R., et al. (2020). Genomewide Association Study of Severe Covid-19 with Respiratory Failure. N. Engl. J. Med.

Elmunzer, B.J., Spitzer, R.L., Foster, L.D., Merchant, A.A., Howard, E.F., Patel, V.A., West,

930   M.K., Qayed, E., Nustas, R., Zakaria, A., et al. (2020). Digestive Manifestations in Patients
931   Hospitalized with COVID-19. Clin. Gastroenterol. Hepatol.

932   Enard, D., and Petrov, D.A. (2018). Evidence that RNA Viruses Drove Adaptive Introgression
933   between Neanderthals and Modern Humans. Cell *175*, 360–371.e13.

934   Enard, D., and Petrov, D.A. (2020). Ancient RNA virus epidemics through the lens of recent
935   adaptation in human genomes. Philos. Trans. R. Soc. Lond. B Biol. Sci. *375*, 20190575.

936   Enard, D., Messer, P.W., and Petrov, D.A. (2014). Genome-wide signals of positive selection in
937   human evolution. Genome Res. *24*, 885–895.

938   Enard, D., Cai, L., Gwennap, C., and Petrov, D.A. (2016). Viruses are a dominant driver of
939   protein adaptation in mammals. Elife *5*, 56.

940   Ferrer-Admetlla, A., Liang, M., Korneliussen, T., and Nielsen, R. (2014). On detecting
941   incomplete soft or hard selective sweeps using haplotype structure. Mol. Biol. Evol. *31*, 1275–
942   1291.

943   Finan, C., Gaulton, A., Kruger, F.A., Lumbers, R.T., Shah, T., Engmann, J., Galver, L., Kelley,
944   R., Karlsson, A., Santos, R., et al. (2017). The druggable genome and support for target
945   identification and validation in drug development. Sci. Transl. Med. *9*.

946   Gene Ontology Consortium (2015). Gene Ontology Consortium: going forward. Nucleic Acids
947   Res. *43*, D1049–D1056.

948   Gordon, D.E., Jang, G.M., Bouhaddou, M., Xu, J., Obernier, K., White, K.M., O'Meara, M.J.,
949   Rezelj, V.V., Guo, J.Z., Swaney, D.L., et al. (2020). A SARS-CoV-2 protein interaction map
950   reveals targets for drug repurposing. Nature *583*, 459–468.

951   Grosse, C., Grosse, A., Salzer, H.J.F., Dünser, M.W., Motz, R., and Langer, R. (2020). Analysis
952   of cardiopulmonary findings in COVID-19 fatalities: High incidence of pulmonary artery thrombi
953   and acute suppurative bronchopneumonia. Cardiovasc. Pathol. *49*, 107263.

954   Hayward, L.K., and Sella, G. (2019). Polygenic adaptation after a sudden change in
955   environment.

956   Hinch, A.G., Tandon, A., Patterson, N., Song, Y., Rohland, N., Palmer, C.D., Chen, G.K., Wang,
957   K., Buxbaum, S.G., Akylbekova, E.L., et al. (2011). The landscape of recombination in African
958   Americans. Nature *476*, 170–175.

959   Hoffmann, C., and Kamps, B.S. (2003). SARS Reference (Flying Publisher).

960   Hormozdiari, F., van de Bunt, M., Segrè, A.V., Li, X., Joo, J.W.J., Bilow, M., Sul, J.H.,
961   Sankararaman, S., Pasaniuc, B., and Eskin, E. (2016). Colocalization of GWAS and eQTL
962   Signals Detects Target Genes. Am. J. Hum. Genet. *99*, 1245–1260.

963   Jeon, S., Blazyte, A., Yoon, C., Ryu, H., Jeon, Y., Bhak, Y., Bolser, D., Manica, A., Shin, E.-S.,
964   Cho, Y.S., et al. (2020). Ethnicity-dependent allele frequencies are correlated with COVID-19
965   case fatality rate (Authorea, Inc.).

966   Kudaravalli, S., Veyrieras, J.-B., Stranger, B.E., Dermitzakis, E.T., and Pritchard, J.K. (2009).
967   Gene expression levels are a target of recent natural selection in the human genome. Mol. Biol.

968 Evol. *26*, 649–658.

969 Luisi, P., Alvarez-Ponce, D., Pybus, M., Fares, M.A., Bertranpetit, J., and Laayouni, H. (2015).
970 Recent positive selection has acted on genes encoding proteins with more interactions within
971 the whole human interactome. Genome Biol. Evol. *7*, 1141–1154.

972 Maclean, C.A., Chue Hong, N.P., and Prendergast, J.G.D. (2015). hapbin: An Efficient Program
973 for Performing Haplotype-Based Scans for Positive Selection in Large Genomic Datasets. Mol.
974 Biol. Evol. *32*, 3027–3029.

975 Michalakis, K., and Ilias, I. (2020). SARS-CoV-2 infection and obesity: Common inflammatory
976 and metabolic aspects. Diabetes Metab. Syndr. *14*, 469–471.

977 Moorjani, P., Sankararaman, S., Fu, Q., Przeworski, M., Patterson, N., and Reich, D. (2016). A
978 genetic method for dating ancient genomes provides a direct estimate of human generation
979 interval in the last 45,000 years. Proc. Natl. Acad. Sci. U. S. A. *113*, 5652–5657.

980 Nédélec, Y., Sanz, J., Baharian, G., Szpiech, Z.A., Pacis, A., Dumaine, A., Grenier, J.-C.,
981 Freiman, A., Sams, A.J., Hebert, S., et al. (2016). Genetic Ancestry and Natural Selection Drive
982 Population Differences in Immune Responses to Pathogens. Cell *167*, 657–669.e21.

983 Ou, X., Liu, Y., Lei, X., Li, P., Mi, D., Ren, L., Guo, L., Guo, R., Chen, T., Hu, J., et al. (2020).
984 Characterization of spike glycoprotein of SARS-CoV-2 on virus entry and its immune cross-
985 reactivity with SARS-CoV. Nat. Commun. *11*, 1620.

986 Piñeiro-Yáñez, E., Reboiro-Jato, M., Gómez-López, G., Perales-Patón, J., Troulé, K.,
987 Rodríguez, J.M., Tejero, H., Shimamura, T., López-Casas, P.P., Carretero, J., et al. (2018).
988 PanDrugs: a novel method to prioritize anticancer drug treatments according to individual
989 genomic data. Genome Med. *10*, 41.

990 Quach, H., Rotival, M., Pothlichet, J., Loh, Y.-H.E., Dannemann, M., Zidane, N., Laval, G.,
991 Patin, E., Harmant, C., Lopez, M., et al. (2016). Genetic Adaptation and Neandertal Admixture
992 Shaped the Immune System of Human Populations. Cell *167*, 643–656.e17.

993 Quintana-Murci, L. (2019). Human Immunology through the Lens of Evolutionary Genetics. Cell
994 *177*, 184–199.

995 Richman, D.D., Whitley, R.J., and Hayden, F.G. (2020). Clinical Virology (John Wiley & Sons).

996 Roberts, G.H.L., Park, D.S., Coignet, M.V., McCurdy, S.R., Knight, S.C., Partha, R., Rhead, B.,
997 Zhang, M., Berkowitz, N., Baltzell, A.K.H., et al. (2020). AncestryDNA COVID-19 Host Genetic
998 Study Identifies Three Novel Loci. medRxiv.

999 Sabeti, P.C., Schaffner, S.F., Fry, B., Lohmueller, J., Varilly, P., Shamovsky, O., Palma, A.,
1000 Mikkelsen, T.S., Altshuler, D., and Lander, E.S. (2006). Positive natural selection in the human
1001 lineage. Science *312*, 1614–1620.

1002 Sattar Naveed, McInnes Iain B., and McMurray John J.V. (2020). Obesity Is a Risk Factor for
1003 Severe COVID-19 Infection. Circulation *142*, 4–6.

1004 Sawyer, S.L., Wu, L.I., Emerman, M., and Malik, H.S. (2005). Positive selection of primate
1005 TRIM5α identifies a critical species-specific retroviral restriction domain. Proc. Natl. Acad. Sci.
1006 U. S. A. *102*, 2832–2837.

1007 Scarpone, C., Brinkmann, S.T., Große, T., Sonnenwald, D., Fuchs, M., and Walker, B.B. (2020).
1008 A multimethod approach for county-scale geospatial analysis of emerging infectious diseases: a
1009 cross-sectional case study of COVID-19 incidence in Germany. Int. J. Health Geogr. *19*, 32.

1010 Schrider, D.R. (2020). Background Selection Does Not Mimic the Patterns of Genetic Diversity
1011 Produced by Selective Sweeps. Genetics *216*, 499–519.

1012 Siepel, A., Bejerano, G., Pedersen, J.S., Hinrichs, A.S., Hou, M., Rosenbloom, K., Clawson, H.,
1013 Spieth, J., Hillier, L.W., Richards, S., et al. (2005). Evolutionarily conserved elements in
1014 vertebrate, insect, worm, and yeast genomes. Genome Res. *15*, 1034–1050.

1015 Speidel, L., Forest, M., Shi, S., and Myers, S.R. (2019). A method for genome-wide genealogy
1016 estimation for thousands of samples. Nat. Genet. *51*, 1321–1329.

1017 Stern, A.J., Wilton, P.R., and Nielsen, R. (2019). An approximate full-likelihood method for
1018 inferring selection and allele frequency trajectories from DNA sequence data. PLoS Genet. *15*,
1019 e1008384.

1020 Stern, A.J., Speidel, L., Zaitlen, N.A., and Nielsen, R. (2020). Disentangling selection on
1021 genetically correlated polygenic traits using whole-genome genealogies. bioRxiv.

1022 Sudlow, C., Gallacher, J., Allen, N., Beral, V., Burton, P., Danesh, J., Downey, P., Elliott, P.,
1023 Green, J., Landray, M., et al. (2015). UK biobank: an open access resource for identifying the
1024 causes of a wide range of complex diseases of middle and old age. PLoS Med. *12*, e1001779.

1025 Szpiech, Z.A., and Hernandez, R.D. (2014). selscan: an efficient multithreaded program to
1026 perform EHH-based scans for positive selection. Mol. Biol. Evol. *31*, 2824–2827.

1027 Tajima, F. (1989). Statistical method for testing the neutral mutation hypothesis by DNA
1028 polymorphism. Genetics *123*, 585–595.

1029 The COVID-19 Host Genetics Initiative (2020). The COVID-19 Host Genetics Initiative, a global
1030 initiative to elucidate the role of host genetic factors in susceptibility and severity of the SARS-
1031 CoV-2 virus pandemic. Eur. J. Hum. Genet. *28*, 715–718.

1032 Uricchio, L.H., Petrov, D.A., and Enard, D. (2019). Exploiting selection at linked sites to infer the
1033 rate and strength of adaptation. Nat Ecol Evol *3*, 977–984.

1034 Voight, B.F., Kudaravalli, S., Wen, X., and Pritchard, J.K. (2006). A map of recent positive
1035 selection in the human genome. PLoS Biol. *4*, e72.

1036 Wong, A.C.P., Li, X., Lau, S.K.P., and Woo, P.C.Y. (2019). Global Epidemiology of Bat
1037 Coronaviruses. Viruses *11*.

1038 World Health Organization (2019). Middle East respiratory syndrome coronavirus (MERS-CoV).

1039 Zeberg, H., and Pääbo, S. (2020). The major genetic risk factor for severe COVID-19 is
1040 inherited from Neandertals.

1041